Organosulfur Precursor for Atomic Layer Deposition of High-Quality Metal Sulfide Films

Hao Li, † Ran Zhao,† Jiahao Zhu,† Zheng Guo, Wei Xiong, Xinwei Wang*

School of Advanced Materials, Shenzhen Graduate School, Peking University, Shenzhen 518055, China

†These authors contributed equally.

*Corresponding email: wangxw@pkusz.edu.cn

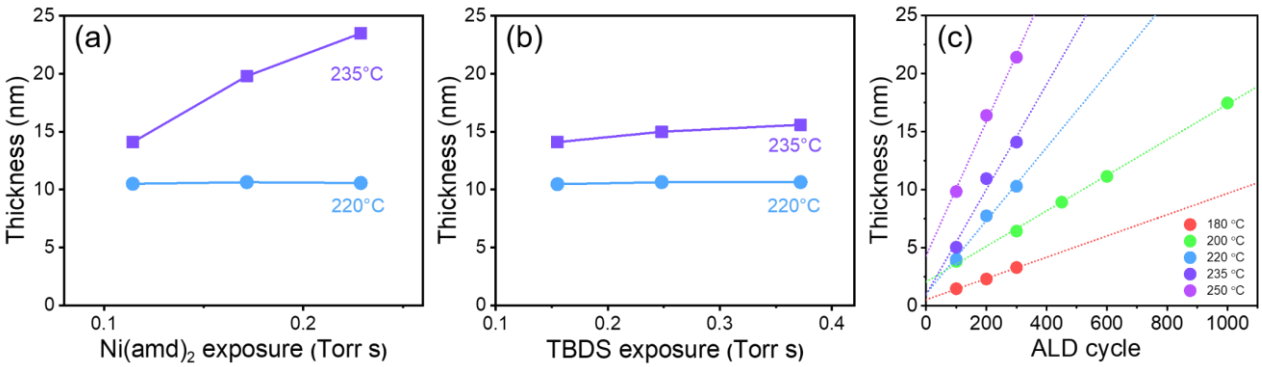

Figure S1. (a,b) NiS_x film growth behavior at 220 and 235 °C: (a) NiS_x film thickness versus the $Ni(amd)_2$ exposure, given a fixed TBDS exposure of ~0.15 Torr s, and (b) NiS_x film thickness versus the TBDS exposure, given a fixed $Ni(amd)_2$ exposure of ~0.12 Torr s. All the films were deposited by 300 ALD cycles. Notably, the growth at 235 °C was no longer saturated. (c) Thickness of the NiS_x films deposited at various temperatures with respect to the number of ALD cycles. The exposures of $Ni(amd)_2$ and TBDS in each ALD cycle were ~0.12 and ~0.15 Torr s, respectively.

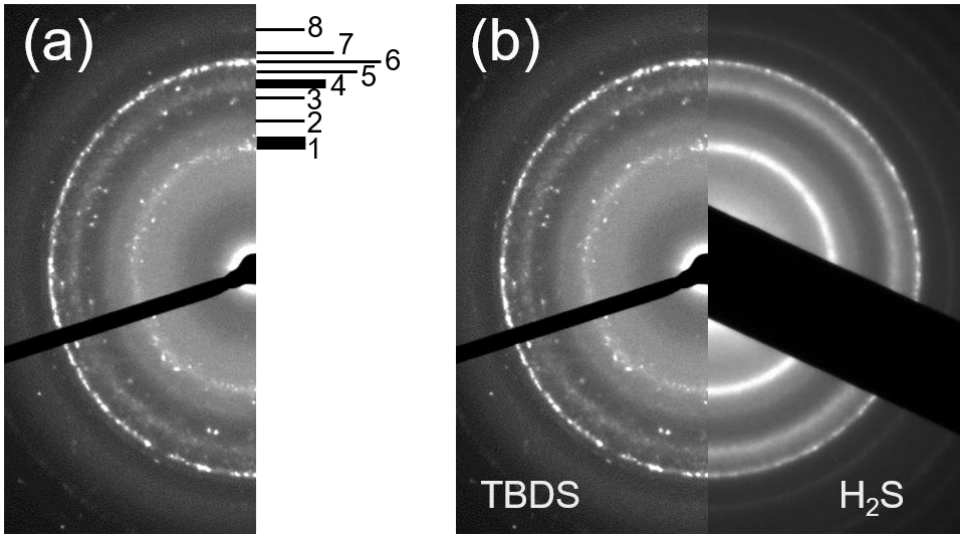

Figure S2. (a) Enlarged view of the diffraction pattern shown in Figure 2b. The labeled numbers are used in Table S1 for indexing the diffraction rings. (see Table S1). (b) Side-by-side comparison of the diffraction patterns for the ALD NiS_x films deposited with TBDS (this work) and H_2S (*Chem. Mater*. **2016**, 28, 1155).

Table S1. Comparison of the d-spacings for the godlevskite Ni_9S_8 structure (PDF #22-1193) and the values measured by TEM. The label numbers in the last column correspond to the labels of the diffraction rings in Figure S2.

PDF # 22-1193			**TEM results**	
(h k l)	d (Å)	Intensity	Measured (Å)	Label number in Figure S2
(222)	2.8500	100.0	2.66-2.82	1
(132)	2.8000	20.0		
(023)	2.7500	20.0		
(203)	2.6200	10.0		
(240)	2.4000	10.0	2.34	2
(330)	2.3700	10.0		
(241)	2.3300	40.0		
(332)	2.1200	10.0	2.10	3
(043)	2.1000	50.0		
(243)	1.9060	30.0	1.82-1.90	4
(115)	1.8320	30.0		
(153)	1.8030	90.0		
(025)	1.7950	80.0		
(261)	1.7140	10.0	1.72	5
(530)	1.6540	80.0	1.62	6
(531)	1.6250	30.0		
(154)	1.6080	10.0	1.58	7
(006)	1.5760	10.0		
(354)	1.4390	20.0	1.42	8
(370)	1.4260	10.0		
(264)	1.3990	10.0		

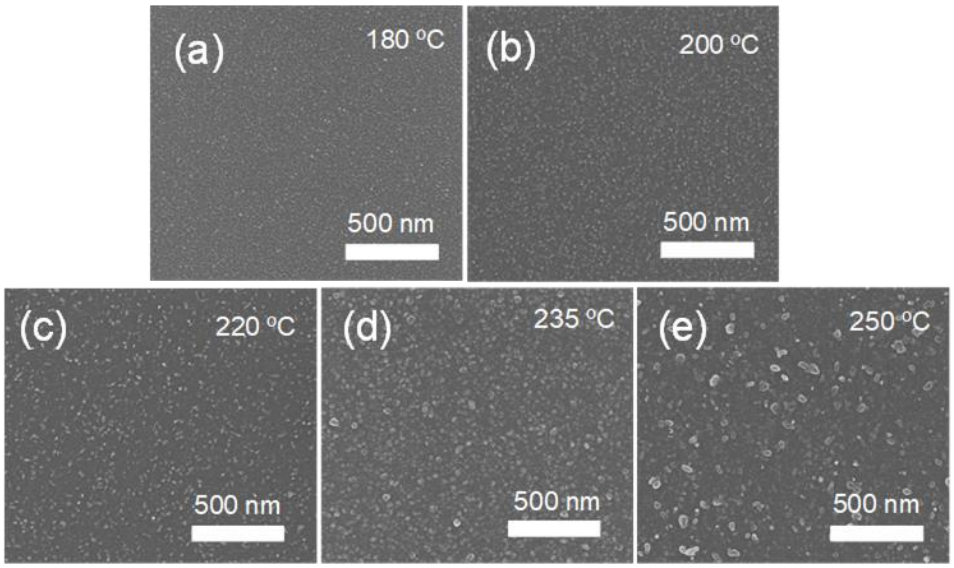

Figure S3. SEM images of ~16 nm ALD NiS_x films deposited at (a) 180 ˚C, (b) 200 ˚C, (c) 220 ˚C, (d) 235 ˚C, and (e) 250 ˚C.

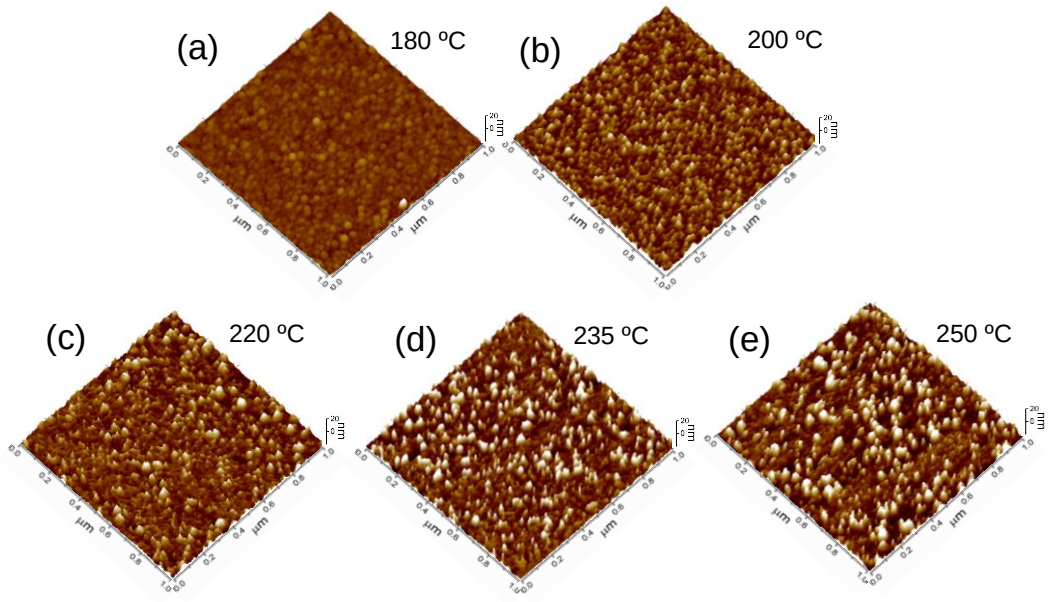

Figure S4. AFM images of ~16 nm ALD NiS_x films deposited at (a) 180 ˚C, (b) 200 ˚C, (c) 220 ˚C, (d) 235 ˚C, and (e) 250 ˚C.

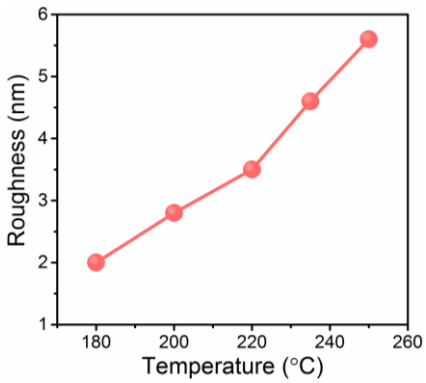

Figure S5. Film surface (rms) roughness with respect to the deposition temperature.

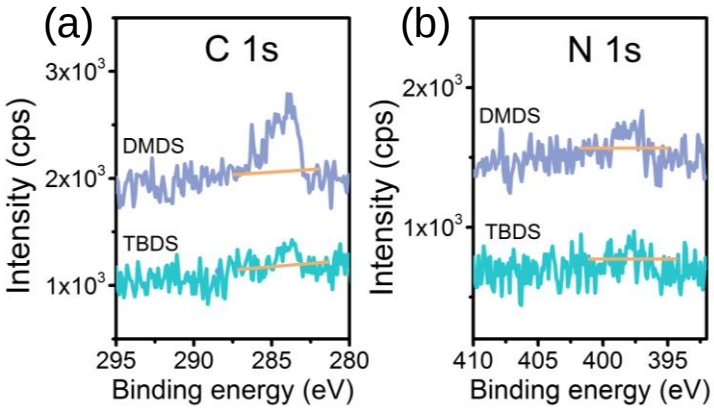

Figure S6. Comparison of the impurities for the ALD NiS_x films deposited using DMDS or TBDS as the sulfur source. (a) C 1s and (b) N 1s XPS spectra taken on 8−10 nm ALD NiS_x films deposited at 200 ˚C. Prior to the XPS data collection, the NiS_x films were subjected to 10 s of Ar^+-ion (3 keV) sputtering to remove surface adventitious carbon. The TBDS curves were reproduced from Figure 2j,k for comparison.

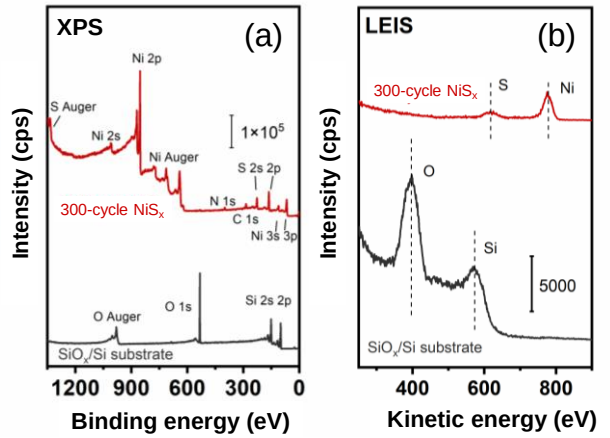

Figure S7. (a) XPS and (b) LEIS spectra collected on a bare SiO_x/Si substrate and the substrate covered by 300 ALD cycles of NiS_x.

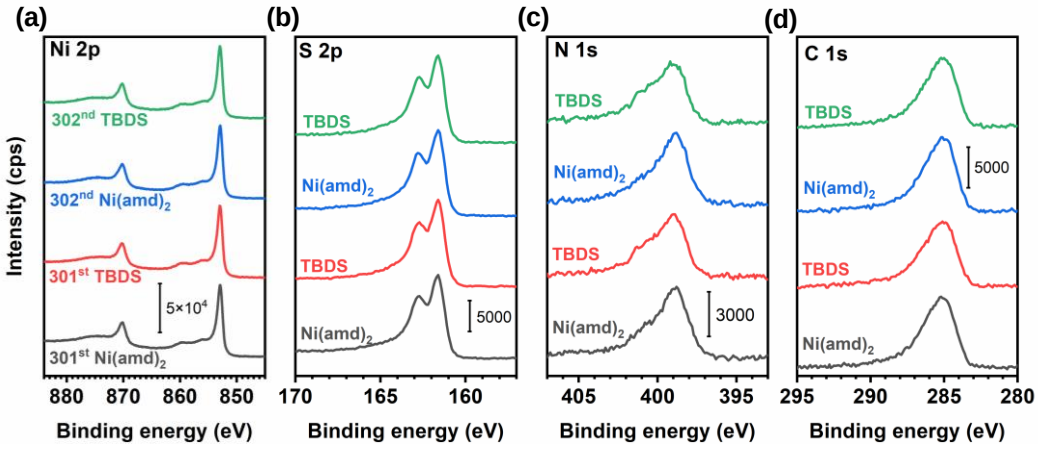

Figure S8. In situ XPS spectra of (a) Ni 2p, (b) S 2p, (c) N 1s, and (d) C 1s taken after the doses of $Ni(amd)_2$ and TBDS in the 301st and 302nd half-cycles. The similarity of the spectra for the 301st and 302nd half-cycles indicates that the data were reproducible.

Table S2. Fitting parameters for the N 1s and C 1s XPS spectra shown in Figure 3d,e

	N 1s									C 1s
	Component 1				Component 2				1+2	TA (cps eV)
	BE (eV)	W (eV)	A (cps eV)	RI (%)	BE (eV)	W (eV)	A (cps eV)	RI (%)	TA (cps eV)	
$Ni(amd)_2$	398.9	1.9	9542.4	74.1	400.9	**1.9**	3339.5	25.9	12881.9	25780.5
TBDS	399.0	1.9	8229.8	68.7	401.0	**1.9**	3748.3	31.3	11978.1	24223.5

* BE= Binding Energy, W= Width, A= Area, RI= Relative Intensity, TA= Total Area. Bold font values stand for fixed parameters.

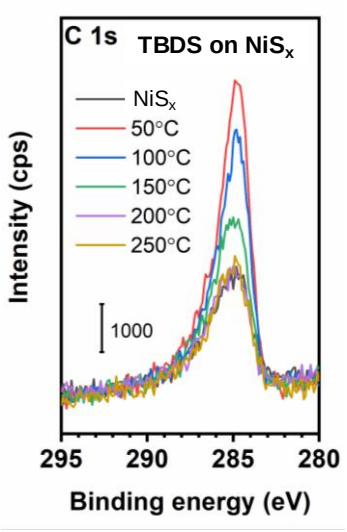

Figure S9. As-collected C 1s XPS spectra for a TBDS-dosed NiS_x substrate subjected to heat treatments at various temperatures. Before dosing TBDS, the NiS_x substrate was annealed at 350 °C to liberate most of the surface organic species, and the XPS spectrum of the annealed NiS_x substrate was used as the background to obtain Figure 4a.

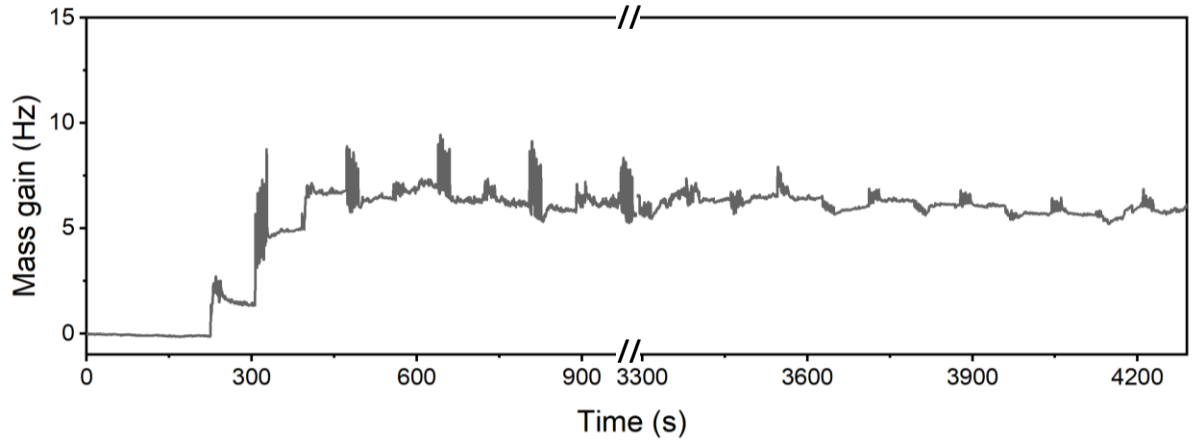

Figure S10. Trace of the in-situ QCM mass gain during the ALD at 150 ˚C.

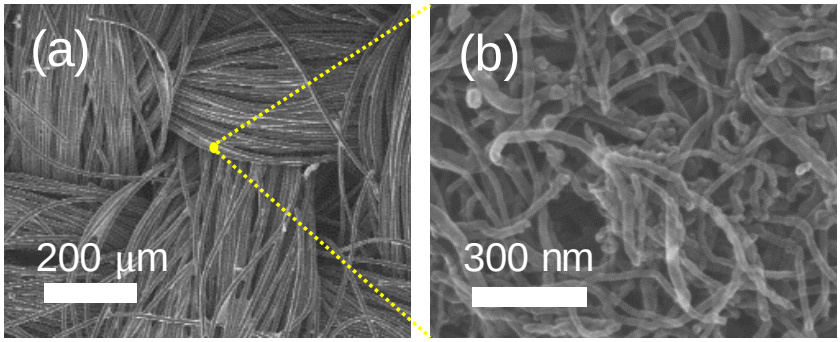

Figure S11. (a) SEM image of the CNT/CC electrode. (b) High-resolution SEM image showing the network of the carbon nanotubes on the carbon cloth.

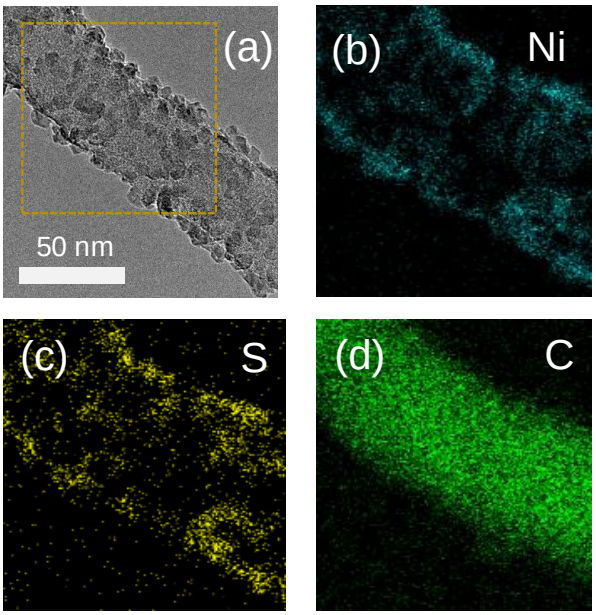

Figure S12. (a) TEM image and the corresponding EDS elemental maps of (b) Ni, (c) S, and (d) C, showing an ~8 nm ALD NiS_x film coated on a carbon nanotube of the CNT/CC electrode.

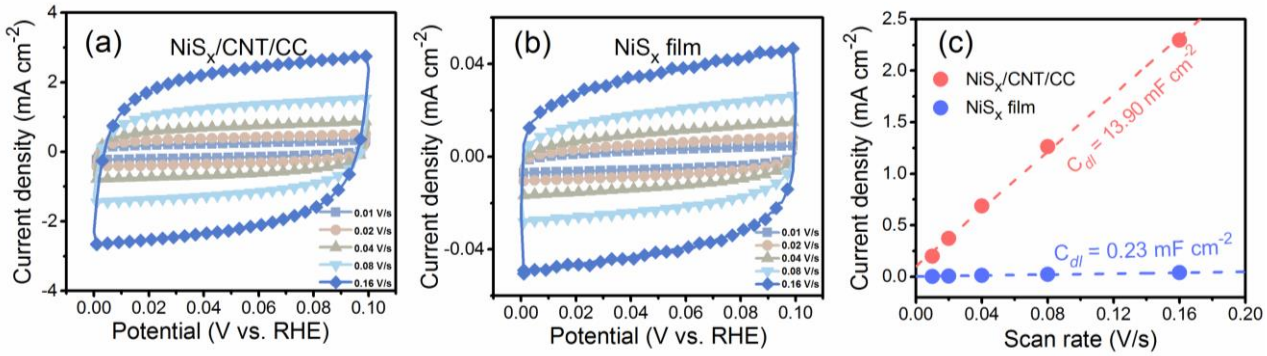

Figure S13. Measurements of the electrode electrochemical double-layer capacitances (C_{dl}) by cyclic voltammetry (CV). CV curves for (a) the NiS_x/CNT/CC and (b) thin-film NiS_x electrodes. The CV scans were conducted in the non-Faradic region of 0 to 0.1 V (vs. RHE) with the scan rates of 0.01, 0.02, 0.04, 0.08, and 0.16 V/s. (c) Plot of the current densities with respect to the scan rate for both electrodes. C_{dl} were extracted from the slopes of the linear fits, to be 13.90 and 0.23 mF cm^{-2} for the NiS_x/CNT/CC and thin-film NiS_x electrodes, respectively. The former was 60.4 times larger than the latter.

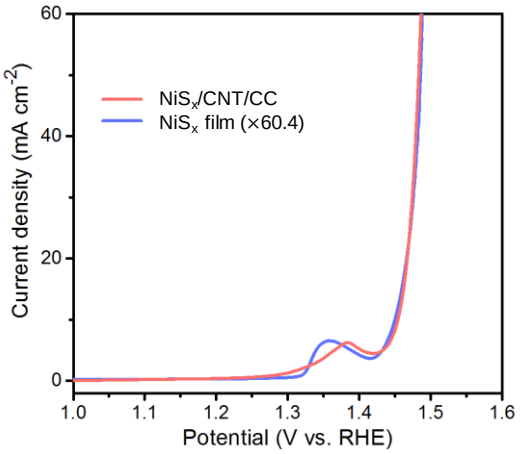

Figure S14. To account for the enlarged surface area of the NiS_x/CNT/CC electrode, the LSV curve of the thin-film NiS_x electrode (Figure 6d) is multiplied by a factor of 60.4. The resultant curve overlaps well with the measured curve of the NiS_x/CNT/CC electrode, which suggests that the enhanced electrocatalytic performance of the NiS_x/CNT/CC electrode was because of the enhancement of the catalyst surface area.

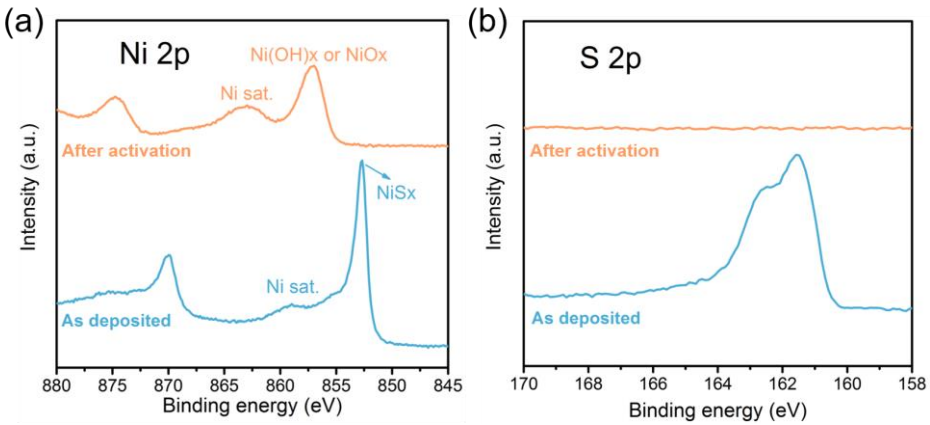

Figure S15. (a) Ni 2p and (b) S 2p XPS spectra for an as-deposited NiS_x/CNT/CC electrode and the electrode after electrochemical activation.

Table S3. Comparison of the OER performance for various reported Ni-based electrocatalysts.

Catalyst	Overpotential (η) @ 10 mA cm^{-2}	Tafel slope (mV/decade)	Reference
NiS_x/CNT/CC	**221**	**48**	**This work**
ALD NiS_x film	**303**	**48**	**This work**
ALD Ni_9S_8 film	353	56	*Chem. Mater.* **2016**, 28, 1155
Ni_3Se_2/Ni foam	270	142.8	*Energy & Environ. Sci.* **2016**, 9, 1771
NiCoP/C nanoboxes	330	96	*Angew. Chem. Int. Ed.* **2017**, 129, 3955
Fe-doped NiO_x nanotubes	310	49	*Nano Energy* **2017**, 38, 167
$NiB_{0.45}$/Cu	296	58	*Nano Energy* **2017**, 38, 175
NGO/Ni_7S_6	381	45	*Adv. Funct. Mater.* **2017**, 27, 1700451
Ni-Ni_3S_2@carbon nanoplates	285	56	*Small* **2019**, 15, 1900348
NiS_x nanoparticles	301	41	*ChemCatChem* **2019**, 11, 1205
$Ni_{0.88}Co_{1.22}Se_4$ hollow microparticles	340	78	*Chem. Mater.* **2017**, 29, 7032
Electrochemically oxidized Ni-sulfide foam	256	41	*Appl. Catal. B* **2018**, 233, 130
$NiFeO_x$	245	34	*ACS Cent. Sci.* **2019**, 5, 3, 558
Ni_3N/Ni_2P/BP	247	78	*J. Mater. Chem. A*, **2019**, 7, 22063
Ni_3S_2 nanosheet array	260	N/A	*J. Am. Chem. Soc.* **2015**, 137, 44, 14023
Ni_2P/carbon paper	280	48	*ACS Catal.* **2017**, 7, 8, 5450
Ni_2P/CoN-porous carbon	270	65	*Chem. Commun.*, **2018**, 54, 12101